Langmuir
Article
pubs.acs.org/Langmuir

Atomic Force Microscopy of Polymer Brushes: Colloidal versus Sharp Tips

A. Halperin*

Laboratoire de Spectrométrie Physique (UMR 5588), Université Joseph Fourier - CNRS, BP 87, 38402 Saint Martin d'Hères, France

E. B. Zhulina

Institute of Macromolecular Compounds of the Russian Academy of Sciences, St. Petersburg, Russia

Received December 16, 2009. Revised Manuscript Received March 26, 2010

Force versus distance profiles acquired by atomic force microscopy probe the structure and interactions of polymer brushes. An interpretation utilizing the Derjaguin approximation and assuming local compression of the brush is justified when colloidal probes are utilized. The assumptions underlying this approach are not satisfied for sharp tips, and deviations from this model were reported for experiments and simulations. The sharp-tip force law proposed assumes that the free energy penalty of insertion into the brush is due to the osmotic pressure of the unperturbed brush. This static force law is in semiquantitative agreement with the simulation results of Murat and Grest (Murat, M.; Grest, G. S. *Macromolecules* **1996**, *29*, 8282).

I. Introduction

Force versus distance profiles obtained via atomic force microscopy (AFM) probe the structure and interactions of polymer brushes[1−11] and of physically adsorbed polymer layers.[12−14] The AFM force curves can be acquired with colloidal probes[8−11] or sharp tips.[1−7] Colloidal probes comprise microspheres, with a radius in the range of 1−30 μm, glued to the cantilever.[15] The sharp tips are typically pyramidal, and their radii of curvature at the apex vary in the range of 2−60 nm with half-cone angles from about 35° to 10°.[15,16] This last category also includes cylindrical carbon nanotube (CNT) tips, having diameters of 1−3 nm for single-walled CNTs (SWNTs).[17,18] The fitting and interpretation of the force profiles often invoke thermodynamic force laws.[2,5−11] These convert the compression force law of a brush confined by a planar boundary to the tip's geometry via the Derjaguin approximation:[15] the force acting on a tip with a rotational symmetry is obtained by summing the contributions of circular, locally flat strips of altitude z assuming that each strip experiences the pressure exerted by a brush compressed by a planar surface at height z. This approximation is justified when the probe−surface separation and the brush height are small in comparison to the probe's radius of curvature. The equilibrium height of a brush, H_{brush}, is typically of order of 10^2 nm. Accordingly, the Derjaguin approximation utilizing the planar force law is reasonable for colloidal probes but questionable for sharp tips. This general observation is supplemented by experimental and simulation results. The experimental results[1−4] suggest that the sharp-tip force laws are shallower than the ones obtained by the surface force apparatus (SFA) where the Derjaguin approximation involving compression is certainly applicable. This effect was attributed to splaying of the polymer chain configurations so as to accommodate a sharp impenetrable tip.[1,19] The experimental observations and their interpretation were also confirmed by computer simulations.[19,20] At present, there is no theoretical expression for the sharp-tip force laws as obtained for swollen brushes using molecular dynamics[19] and Monte Carlo simulations.[20] Theoretical studies considered molten brushes[21,22] and swollen brushes probed by wide-based cylindrical tips.[23] Accordingly, the Derjaguin approximation assuming compression of the brush is utilized to describe sharp tip force profiles because of the current lack of an alternative approach.[2,5−7] In the following, we propose a phenomenological theory of the interactions between sharp tips and polymer brushes yielding simple analytical expressions for the thermodynamic sharp-tip force law. It estimates the free energy penalty associated with the insertion of a sharp AFM tip into the brush by the work expended against the osmotic pressure of the *unperturbed* brush. The Derjaguin approximation is not utilized. Within this view, the insertion of the sharp tip does not give rise to compression of the brush. Rather, it produces a

*To whom correspondence should be addressed. E-mail: avraham.halperin@ujf-grenoble.fr.

(1) O'Shea, S. J.; Welland, M. E.; Rayment, T. *Langmuir* **1993**, *9*, 1826–1835.
(2) Lea, A. S.; Andrade, J. D.; Hlady, V. *Colloids Surf., A* **1994**, *93*, 349–357.
(3) Overney, R. M.; et al. *Phys. Rev. Lett.* **1996**, *76*, 1272–1275.
(4) Kelley, T. W.; Schorr, P. A.; Johnson, K. D.; Tirrell, M.; Frisbie, C. D. *Macromolecules* **1998**, *31*, 4297–4300.
(5) Butt, H-J; Kappl, M; Mueller, H; Raiteri, R; Meyer, W.; Rühe, J *Langmuir* **1999**, *15*, 2559–2565.
(6) Nnebe, I. M.; Schneider, J. W. *Macromolecules* **2006**, *39*, 3616–3621.
(7) Mendez, S.; et al. *Langmuir* **2009**, *25*, 10624–10632.
(8) Yamamoto, S; Ejaz, M; Tsujii, Y.; Matsumoto, M; Fukuda, T *Macromolecules* **2000**, *33*, 5602–5607.
(9) Musoke, M; Luckham, P. F. *J. Colloid Interface Sci.* **2004**, *277*, 62–70.
(10) McLean, S. C.; Lioe, H; Meagher, L; Craig, V. S. J.; Gee, M. L. *Langmuir* **2005**, *21*, 2199–2208.
(11) Nnebe, I. M.; Tilton, R. D.; Schneider, J. W. *J. Colloid Interface Sci.* **2004**, *276*, 306–316.
(12) Biggs, S *Langmuir* **1995**, *11*, 156–162.
(13) Braithwaite, C. J. C.; Howe, A; Luckham, P. F. *Langmuir* **1996**, *12*, 4224–4237.
(14) Meagher, L; Maurdev, G.; Gee, M. L. *Langmuir* **2002**, *18*, 2649–2657.
(15) Butt, H.-J.; Cappella, B.; Kappl, M. *Surf. Sci. Rep.* **2005**, *59*, 1–152.
(16) Barattin, R.; Voyer, N. *Chem. Commun.* **2008**, 1533–1532.
(17) Hafner, J. H.; Cheung, C.-L.; Wolley, A. T.; Lieber, C. M. *Prog. Biophys. Mol. Biol.* **2001**, *77*, 73–110.
(18) Wilson, N. R.; Macpherson, J. V. *Nat. Nanotechnol.* **2009**, *4*, 483–491.
(19) Murat, M; Grest, G. S. *Macromolecules* **1996**, *29*, 8282–8284.
(20) Jimenez, J.; Rajagopalan, R. *Eur. Phys. J. B* **1998**, *5*, 237–243.
(21) Fredrickson, G. H.; Ajdari, A.; Leibler, L.; Carton, J.-P. *Macromolecules* **1992**, *25*, 2882–2889.
(22) Williams, D. R. M. *Macromolecules* **1993**, *26*, 5096–5098.
(23) Subramanian, G.; Williams, D. R. M.; PincusP, A. *Macromolecules* **1996**, *29*, 4045–4050.

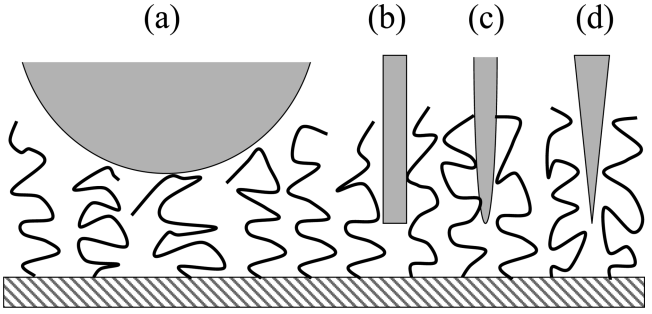

Figure 1. Compressive versus insertive modes. Large colloidal probe (a) approachs the surface by compressing the brush. In contrast, sharp tips, exemplified by cylindrical (b), paraboloid (c), and conical tips (d), perturb the brush only locally.

short ranged perturbation of the brush concentration profile in the vicinity of the tip, as suggested by the simulation results.[19,24] This view is analogous to the model invoked for the insertion of small globular proteins into the brush.[25−27] As we shall see, the force law thus obtained is in semiquantitative agreement with the simulation results. While our discussion focuses on polymer brushes, the approach can be used to describe the interactions between sharp tips and layers of adsorbed homopolymers, swollen gels, and so on. For simplicity, we limit the analysis to nonadsorbing tips having rotational symmetry and to swollen brushes exhibiting mean field (MF) behavior, that is, marginal good solvents and Θ solvents. To explore the role of tip geometry we compare the force laws of cylindrical, paraboloid, and conical tips. For comparison purposes, we also discuss the corresponding force laws as obtained upon assuming local confinement and invoking the Derjaguin approximation. We emphasize that the thermodynamic force laws are obtained assuming a stationary tip immersed in an equilibrated brush. Accordingly, they apply when the brush relaxation is fast in comparison with the motion of the tip. We shall return to this issue in the Discussion.

Overall, it is helpful to distinguish two extreme scenarios of the approach of AFM tip toward a polymer brush (Figure 1). In the compressive limit, realized by colloidal probes, the brush is locally confined. This gives rise to a modified concentration profile with a higher monomer density. Within this scenario, the force profile reflects, as we shall discuss, the local osmotic pressure of the compressed brush at the boundary of the tip. In the insertion limit, as realized by sharp tips, the overall brush structure is only weakly modified and the force profile reflects the osmotic pressure in the unperturbed brush. Clearly, both views are approximations of interest because they yield analytical expressions allowing to fit and interpret experimental and simulation data. With this caveat in mind, it is of interest to note two features that distinguish the insertion and compressive modes: (i) The compressive mode force laws diverge for deep insertions because of the densification of the brush by the tip. In contrast, the force associated with the insertion limit does not diverge because the osmotic pressure of the unperturbed brush is always finite. (ii) The insertion mode clearly distinguishes between brushes modeled by steplike concentration profiles and brushes having a parabolic concentration profile. In contrast, the compressive force law can be fitted by the two brush models.[28]

The remainder of the paper is organized as follows. General features of the insertion mode force law are described in section II. It specifies the expressions for calculating the insertion free energy and the corresponding force law as well as their compressive mode counterparts. The underlying approximations and their range of applicability are also described. Certain aspects of the detailed discussion concerning the compressive force law within the self-consistent field (SCF) theory and the insertive case in the Alexander model are delegated to Appendix I and II, respectively. The insertion mode force laws for cylindrical, paraboloid and conical tips, as obtained for marginal and Θ solvents, are described in section III. For comparison purposes we present, in section IV, the force laws obtained for identical tips in the compressive limit, upon utilizing the Derjaguin approximation. The applicability of the static sharp-tip force laws, as determined by the tip's form and approach velocity, is briefly discussed in the Discussion. Technical aspects of sections II and IV are discussed in Appendix III.

II. The Insertion Penalty: General Considerations

The main thrust of this work concerns explicit force profiles of inserting AFM sharp tips into polymer brushes. In this section, we first describe the approach and then discuss the underlying physics, the regime of applicability, and the approximations involved. To obtain explicit force laws, we consider brushes exhibiting MF behavior. In other words, the chains exhibit Gaussian elasticity and the free energy density of monomer−monomer interactions, kTf_{inter} is given by the virial expansion $f_{\mathrm{inter}} = \tau a^3 c^2 + w a^6 c^3 + ... = (\tau\phi^2 + w\phi^3 + ...)/a^3$ where $ca^3 = \phi$ is the monomer volume fraction and a is a monomer size. Here $v \approx \tau a^3$ is the second virial coefficient, $\tau = (T - \Theta)/T$ is a reduced temperature characterizing the deviation from the Θ temperature, the third virial coefficient is $wa^6 = \mathrm{const}'$, and k is the Boltzmann constant. The MF regime is realized for brushes of semiflexible chains with persistence length $l_p \approx pa$ such that $1 < p \ll N$ when $\Sigma \lesssim p^4/\tau^2$.[29] In this regime, the SCF theory yields analytical expressions for the concentration profiles of the brush, $\phi(z)$[30−32] (Appendix I). In turn, these yield explicit expressions for the local osmotic pressure $\Pi(z) = \phi(\partial f_{\mathrm{inter}}/\partial\phi) - f_{\mathrm{inter}}$ of a bulk solution with $\phi = \phi(z)$. Within the brush, $\Pi(z)$ specifies the lateral pressure[30] (Appendix II). With these ingredients at hand, we identify the free energy penalty of insertion of a sharp tip with the work expended against $\Pi(z)$ of the *unperturbed* brush

$$F_{\mathrm{ins}} = \int_D^{H_{\mathrm{brush}}} \Pi(z)\, A(z)\, \mathrm{d}z \qquad (1)$$

Here, $A(z)$ is the cross-sectional area of the tip at z, D is the altitude of the tip's apex, and H_{brush} is the equilibrium height of the unperturbed brush. The corresponding force law is thus

$$f_{\mathrm{ins}} = -\frac{\partial}{\partial D}\int_D^{H_{\mathrm{brush}}} \Pi(z)\, A(z)\, \mathrm{d}z \qquad (2)$$

We obtain explicit force laws for marginal good solvents, when $f_{\mathrm{inter}} \approx \tau\phi^2/a^3$ leading to $\Pi(z)a^3/kT \approx \tau\phi(z)^2$, and for Θ solvents, where $f_{\mathrm{inter}} \approx w\phi^3/a^3$ and $\Pi(z)a^3/kT \approx 2w\phi(z)^3/a^3$. To this end, we

(24) Ermilov V.; Lazutin A.; Halperin A. *Macromolecules* **2010**, *43*, 3511−3520.
(25) Halperin, A. *Langmuir* **1999**, *15*, 2525–2533.
(26) Halperin, A.; Fragneto, G.; Schollier, A.; Sferrazza, M. *Langmuir* **2007**, *23*, 10603–10617.
(27) Halperin, A; Kröger, M *Langmuir* **2009**, *25*, 11621–11634.
(28) Taunton, H. J.; Toprakcioglu, C.; Fetters, L. J.; Klein, J. *Macromolecules* **1990**, *23*, 571.
(29) Birshtein, T. M.; Zhulina, E. B. *Polymer* **1984**, *25*, 1453–1461.
(30) Milner, S. T.; Witten, T. A.; Cates, M. E. *Macromolecules* **1988**, *21*, 2610–1619.
(31) Zhulina, E. B.; Borisov, O. V.; Priamitsyn, V. A. *J. Colloid Interface Sci.* **1990**, *137*, 495–511.
(32) Milner, S. T. *Science* **1991**, *251*, 905–914.

utilize the SCF concentration profiles[31] (Appendix I)

$$\phi(z) = \begin{cases} \phi_0\left(1-\dfrac{z^2}{{H_0}^2}\right) & \text{marginal solvent} \\ \phi_\theta\left(1-\dfrac{z^2}{{H_\theta}^2}\right)^{1/2} & \Theta \text{ solvent} \end{cases} \quad (3)$$

Here, ϕ_0 and ϕ_Θ denote the monomer volume fraction at the grafting surface for marginal and Θ solvents, respectively, and the corresponding brush heights are H_0 and H_Θ:

$$\phi_0 = \frac{3\pi^{2/3}}{4(\tau p)^{1/3}}\left(\frac{a^2}{\Sigma}\right)^{2/3} \quad H_0 = \left(\frac{8}{\pi^2}\right)^{1/3}(\tau p)^{1/3}\left(\frac{a^2}{\Sigma}\right)^{1/3} Na$$

$$\phi_\Theta = \frac{2}{(wp)^{1/4}}\left(\frac{a^2}{\Sigma}\right)^{2/3} \quad H_\Theta = \frac{4}{\pi}\left(\frac{wp}{2}\right)^{1/4}\left(\frac{a^2}{\Sigma}\right)^{1/3} Na \quad (4)$$

As noted earlier, F_{ins} is actually the work expended to oppose the "lateral osmotic pressure" in the brush, Π_{lat}. In brushes exhibiting MF behavior, $\Pi_{lat}(z) = \Pi(z)$, while in athermal solvent $\Pi_{lat}(z) = 8\Pi(z)/7$. In the following, we focus on the MF case where analytical solutions of $\phi(z)$ lead to simple expressions for the force profiles.

As stated earlier, our analysis concerns sharp tips that approach the brush coated surface without compressing the brush. This insertive mode is realized for small particles while large particles follow the compressive mode. The definition of large and small depends on the form of the particle. For a sphere of radius R_p, the crossover between two regimes is defined in terms of H_{brush}. The compressive regime occurs for $R_p \gg H_{brush}$, while the insertive regime occurs for $R_p \ll H_{brush}$. In physical terms, the distinction arises because chain trajectories circumventing the particle are realizable only for $R_p \ll H_{brush}$.[33] In the case of cylindrical tips, whose overall height L is larger than H_{brush}, the crossover as observed in simulations occurs roughly at $r_{cyl} \approx R_0$, where $R_0 \approx N^{1/2}a$ is the lateral span of a grafted chain in a brush.[19] When $r_{cyl} \gg R_0$, the chains between the tip and the surface are confined and the force law approaches the force profile of compression by a planar surface. In the opposite limit, the splayed chains configurations circumvent the tip, and the force profile is much shallower.

The insertive force law is traceable to $\Pi(z)$ of the unperturbed brush. For compression by an infinite planar piston, the known force profile within the SCF theory[30,31] is also traceable to the Π of the brush (Appendix I):

$$P_{planar} = \Pi[\phi_{confined}(H)] \quad (5)$$

However, in this case, $\Pi[\phi_{confined}(H)]$ is Π of the confined brush at the impenetrable boundary at height $H < H_{brush}$, where the local volume fraction is $\phi = \phi_{confined}(H)$. Accordingly, the compressive force profile of a tip within the Derjaguin approximation is

$$f_{comp} = \int_{A(D)}^{A(H_{brush})} \Pi[\phi_{confined}(z)]\, dA(z) \quad (6)$$

Thus, while both force laws are traceable to Π, in the insertive case it is $\Pi(z)$ of the unperturbed brush while in the compressive case it is Π at the edge of the confined brush.

At this point, it is useful to comment on the utility of the Alexander model[34] for obtaining force laws. For weak compressions, it leads to harder repulsion in comparison to the SCF compressive force law.[30,31] In addition, it does not lead to $P_{planar} = \Pi[\phi_{confined}(H)]$ obtained in the SCF theory (Appendix I). With these caveats, The Alexander model allows one to successfully fit SFA force profiles[28] where the compressive regime is certainly operative. In marked contrast, it leads to qualitatively wrong results for the insertive force profile. Since it assumes a steplike concentration profile, ϕ within the brush is constant and so is Π. For cylindrical tips of cross-sectional area A_{cyl}, the insertion mode for the Alexander model leads to $F_{ins} = A_{cyl}(H_{brush} - D)\Pi$. Accordingly, the force law is $f_{ins} = -\partial F_{ins}/\partial D = A_{cyl}\Pi = \text{const}'$, in qualitative disagreement with the simulation results of Murat and Grest.[19]

Note that F_{ins} as discussed above does not allow for surface effects. In bulk solutions, the insertion of a nonadsorbing particle incurs free energy penalty comprising two contributions $F_{ins}^{bulk} = \Pi(\phi)V_p + \gamma(\phi)S_p$.[35] Here, $\Pi(\phi)V_p$ is the osmotic work expended upon insertion of a particle of volume V_p. $\gamma(\phi)$ is the surface tension due to the formation of depletion layer at the particle solution interface, $\gamma(\phi)S_p$ is the work associated with its creation, and S_p is the surface area of the particle. A similar situation is expected in the brush. For simplicity, our analysis ignores surface effects. The range of validity regime of this $F_{ins} \approx \Pi(\phi)V_p$ estimate is particularly transparent in athermal solvents when both $\Pi(\phi)$ and $\gamma(\phi)$ are determined by the blob size $\xi \simeq a\phi^{-3/4}$,[36,37] with $\Pi(\phi) \simeq kT/\xi^3$ [36,37] and $\gamma(\phi) \simeq kT/\xi^2$.[38] For sharp tips, it is of interest to consider F_{ins} of cylinders and cones. Neglecting numerical prefactors as well as the contribution of the basal area, and denoting the basal radius by R and the height by L, leads to

$$\frac{F_{ins}^{bulk}}{kT} \simeq \begin{cases} \dfrac{{R_{cyl}}^2 L_{cyl}}{\xi^3}\left[1+\left(\dfrac{\xi}{R_{cyl}}\right)\right] & \text{cylinder} \\ \dfrac{{R_{cone}}^2 L_{cone}}{\xi^3}\left[1+\left(\dfrac{\xi\cos\theta}{R_{cone}}\right)\right] & \text{cone} \end{cases} \quad (7)$$

where θ is the apex half angle of the cone. Accordingly, for these two cases, $F_{ins}^{bulk} = \Pi(\phi)V_p$ is a reasonable estimate when the basal radius is large compared to the blob size, $\xi/R_{cyl} \ll 1$ or $\xi\cos\theta/R_{cone} \ll 1$. This suggests that the surface tension contribution may play a role for certain sharp tips, such as CNT probes. One should also note that surface effects such as ordering and depletion are not well described by the SCF theory we use. We finally emphasize that the discussion of surface effects requires modification when the polymers adsorb to the tip.

III. The Insertion Mode of Sharp Tips

The force on the tip within the insertion case, as specified by eq 2, assumes its simplest form for a straight cylinder with radius r_{cyl} such that the tip's cross section is disklike with an area

(33) Steels, B. M.; Koska, J.; Haynes, C. A. *J. Chromatogr. B* **2000**, *743*, 41–56.
(34) Alexander, S. *J. Phys.* (*Paris*) **1977**, *38*, 977.
(35) Louis, A. A.; Bolhuis, P. G.; Meijer, E. J.; Hansen, J. P. *J. Chem. Phys.* **2002**, *116*, 10547.
(36) de Gennes, P.-G. *Scaling Concepts in Polymer Physics*; Cornell University Press: Ithaca, NY, 1979.
(37) Grosberg, A.Yu.; Khokhlov, A. R. *Statistical Physics of Macromolecules*; American Institute of Physics: New York, 1994.
(38) de Gennes, P. G. *C. R. Acad. Sci. Paris, Ser. B* **1979**, *288*, 359.
(39) Rubinstein, M.; Colby, R. H. *Polymer Physics*; Oxford University Press: Oxford, 2003.

$A_{cyl} = \pi r_{cyl}^2$ irrespective of z or D. Accordingly, $f_{ins} = -A_{cyl}(\partial/\partial D)\int_D^{H_{brush}} \Pi(z)\, dz = A_{cyl}\Pi(D)$. Since the osmotic pressure at the apex, $\Pi(D)$, and H_{brush} depend on the solvent quality, we obtain

$$f_{ins} = \begin{cases} A_{cyl}\Pi_0\left(1 - q_0^2\right)^2 & \text{marginal solvent} \\ A_{cyl}\Pi_\Theta\left(1 - q_\Theta^2\right)^{3/2} & \Theta \text{ solvent} \end{cases} \quad (8)$$

where $q_0 = D/H_0$ and $q_\Theta = D/H_\Theta$. Here, the osmotic pressure at $z = 0$ for a marginal solvent is $\Pi_0 a^3/kT = \tau\phi_0^2$, whereas for a Θ solvent it is $\Pi_\Theta a^3/kT = 2w\phi_\Theta^3$.

For conical and paraboloid tips, where $A(z = D) = 0$, the insertive force is $f_{ins} = -\int_D^{H_{brush}} \Pi(z)\,(\partial A(z)/\partial D)dz$. The force law for a marginal solvent is thus of the form $f_{ins} = A_i^0\Pi_0\psi_i^0(q)$ (Appendix III). Here, A_i^0 is the basal area of a tip fully immersed in a brush swollen by a good solvent, with its apex at the surface, and $\psi_i^0(q_0)$ is a polynomial of q_0. For a cone with an apex half angle Θ, the basal area is $A_{cone}^0 = \pi H_0^2 \tan^2\theta$, while for paraboloid with tip curvature R the basal area is $A_{para}^0 = 2\pi R H_0$. Altogether

$$f_{ins} = \begin{cases} A_{cone}^0\Pi_0 2\left(\frac{1}{6} - \frac{8}{15}q_0 + \frac{q_0^2}{2} - \frac{q_0^4}{6} + \frac{q_0^6}{30}\right) \\ \quad \text{cone, marginal solvent} \\ A_{para}^0\Pi_0\left(\frac{8}{15} - q_0 + \frac{2q_0^3}{3} - \frac{q_0^5}{5}\right) \\ \quad \text{paraboloid, marginal solvent} \end{cases} \quad (9)$$

In a Θ solvent, the force laws assume the form $f_{ins} = A_i^\Theta\Pi_\Theta\psi_i^\Theta(q)$, where the three factors retain their physical significance but adopt different forms. In particular

$$f_{ins} = \begin{cases} A_{cone}^\Theta\Pi_\Theta\frac{1}{20}\left[\left(8 + 9q_\Theta^2 - 2q_\Theta^4\right)\sqrt{1 - q_\Theta^2} - 15q_\Theta \arccos q_\Theta\right] \\ \quad \text{cone } \Theta \text{ solvent} \\ A_{para}^\Theta\Pi_\Theta\frac{1}{8}\left[3\arccos q_\Theta - q_\Theta\left(5 - 2q_\Theta^2\right)\sqrt{1 - q_\Theta^2}\right] \\ \quad \text{paraboloid } \Theta \text{ solvent} \end{cases} \quad (10)$$

where the immersed areas are modified to $A_{cone}^\Theta = \pi H_\Theta^2\tan^2\theta$ and to $A_{para}^\Theta = 2\pi R H_\Theta$ because the brush height in a Θ solvent is lower. For cylindrical tips, in contrast to conical and paraboloid ones, $A_{cyl}^0 = A_{cyl}^\Theta = A_{cyl}$ irrespective of the solvent quality. Importantly, f_{ins} for the insertion mode is finite, irrespective of the tip geometry or solvent quality. However, the $\psi(q)$ plots associated with the various tip shapes differ significantly in their $\psi(0)$ values such that $\psi_{cyl}(0) > \psi_{para}(0) > \psi_{cone}(0)$ (Figure 2).

The performance of these force laws is best judged upon comparison to the simulation results of Murat and Grest.[19] For $(a^2/\Sigma) = 0.1$, v = 1, and $p = 1$, roughly corresponding to the simulation conditions,[19] $\Pi_0 \simeq 0.12kT/a^3$. For these paramters, the force law for a cylindrical tip, as specified by eq 8, is in semiquantitative agreement with the simulation results. The small deviations from the simulations results may be attributed to three factors: (i) Equation 8 was obtained for marginal solvent, while the simulations involved an athermal solvent. (ii) The derivation of eq 8 overlooks surface effects. (iii) The cylindrical tips only approximate the simulations where the cylinders carried spherical caps. For these parameters, it is also of interest to comment on the experimental potential of carbon nanotube tips as realization of cylindrical probes.[17,18] Commercially available CNT probes are characterized by $r_{cyl} = 0.6$ nm for SWNT and $r_{cyl} = 1.2$ nm for double-walled CNT.[40] The associated force scale $A_{cyl}\Pi_0$ is, respectively, 22 and 90 pN, thus suggesting the feasibility of their use to probe polymer brushes and similar polymer layers.

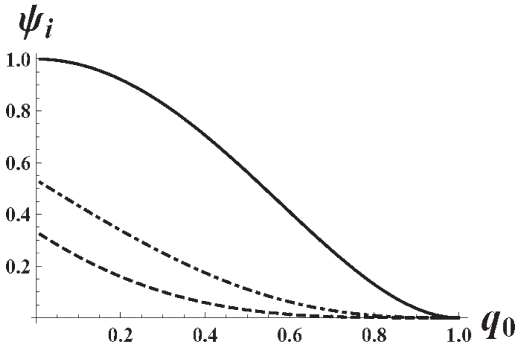

Figure 2. Reduced force profile in the insertive mode in a marginal solvent, $f_{ins}/A_i^0\Pi_0 = \psi_i^0(q)$ versus the reduced insertion depth $q_0 = D/H_0$, for cylindrical (continuous), paraboloid (dot-dashed), and conical (dashed) tips.

IV. The Compression Mode of Sharp Tips: The Derjaguin Approximation

It is instructive to compare the insertive force laws with their compressive counterparts. We limit the discussion to marginal solvents where analytical results are available. The Θ solvent force laws can be obtained numerically (Appendix I). For marginal solvents, the free energy per chain of a brush confined by a planar surface at altitude H is $F_{planar} = (5/9)F_0[t^2 + 1/t - t^5/5]$, where $t = H/H_0$ and $F_0 = kT(9\pi^{2/3}/10)(\tau^2/p)^{1/3}(a^2/\Sigma)^{2/3}N$ is the free energy per chain in the unperturbed brush[31] (Appendix I). The pressure exerted by the compressed brush is thus

$$P_{planar} = -\frac{\partial F_{planar}}{\Sigma\partial H} = P_0\left(\frac{1}{t} - t^2\right)^2 \quad (11)$$

where $P_0 = 5F_0/9\Sigma H_0 = 4\Pi_0/9$ is the pressure scale. The Derjaguin approximation for the "compressive" force experienced by a right cylinder tip with a basal area $A_{cyl} = \pi r_{cyl}^2$ is $f_{comp} = A_{cyl}P_{planar}$ or

$$f_{comp} = A_{cyl}P_{planar} = A_{cyl}P_0\left(\frac{1}{q} - q_0^2\right)^2 \quad \text{cylinder} \quad (12)$$

For conical and paraboloid geometries, the force on the tip is $f_{comp} = \int_{A(D)}^{A(H_0)} dA(z)\, P_{planar}(z)$, where $dA(z)$ of a cone is $dA(z) = 2\pi(z - D)\tan^2\theta\, dz$ while for a paraboloid it is $dA(z) = 2\pi R\, dz$ (Appendix III). f_{comp} assumes the form $f_{comp} = A_i^0P_0\alpha^0{}_i(q_0)$, where A_i^0 is the geometry specific basal area of the fully inserted tip, as discussed in section III, and $\alpha^0{}_i(q_0)$ is a geometry dependent function.

$$f_{comp} = \begin{cases} A_{cone}^0P_0 2\left(-\frac{3}{2} + \frac{9q_0}{5} - \frac{q_0^3}{3} + \frac{q_0^6}{30} - \ln\, q_0\right) & \text{cone} \\ A_{para}^0P_0\left(-\frac{9}{5} + \frac{1}{q_0} + q_0 - \frac{q_0^5}{5}\right) & \text{paraboloid} \end{cases} \quad (13)$$

(40) Available from Nanosensors at http://www.nanosensors.com/prod_cat_sss.html.

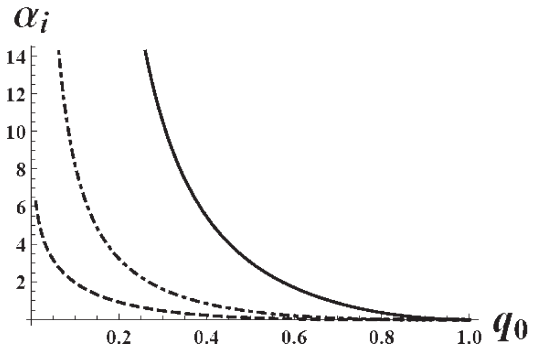

Figure 3. Reduced force profile in the compressive mode in marginal solvent, $f_{comp}/A_i^0 P_0 = \alpha_i^0(q_0)$ versus the reduced insertion depth $q_0 = D/H_0$, for cylindrical (continuous), paraboloid (dot-dashed), and conical (dashed) tips.

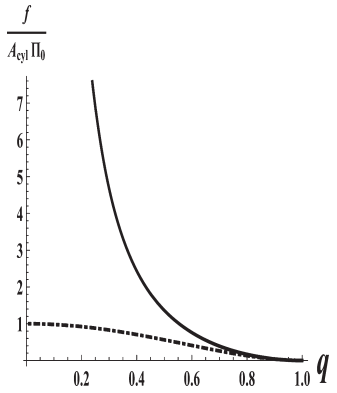

Figure 4. Reduced force law of cylindrical tips, $f/A_{cyl}^0\Pi_0$ versus $q_0 = D/H_0$, in the compressive (continuous) and insertive (dot-dashed) modes.

In contrast to the f_{ins} obtained for the insertion mode, f_{comp} in the compressive mode diverges for deep insertions, as $D \to 0$. As expected, the divergence is steeper for cylinders than for paraboloids, with it being weakest for cones (Figure 3). Yet, irrespective of the geometry, this feature leads to qualitatively different behavior in comparison to the insertion mode (Figure 4).

V. Discussion

Within our discussion, AFM force force profiles fall into two categories. Large tips, as realized by colloidal probes, compress the brush upon approaching the surface, and their force profile is obtainable by the Derjaguin approximation. Sharp tips approach the surface while inducing a short ranged perturbation, and their insertion is opposed by the osmotic pressure of the unperturbed brush. In this case, the static force law is obtained without recourse to the Derjaguin approximation. The insertion mode rationalizes experimental observations and simulation results showing that the AFM force profile obtained with sharp tips is shallower than the force law observed in SFA experiments. In qualitative terms, the two force laws differ because the compressive force profiles diverge for deep penetrations while the insertion force profiles do not. For marginal and Θ solvents, the insertion mode force laws assume a simple analytical form. These are attained at the price of neglecting surface effects and utilizing SCF results with their underlying assumptions. They enable however fitting and interpretation of sharp tip AFM force profiles as obtained experimentally or via simulations.

Care should be taken in applying the static sharp tip force laws. Two questions are involved: First, is the tip motion slow enough to justify the use of a static force law derived from thermodynamics? Second, is the tip utilized sharp in the sense that its insertion induces only a short-range perturbation of the brush? The first question was theoretically analyzed for the case of SFA by Fredrickson and Pincus[41] focusing on the role of hydrodynamic lubrication. For a brush swollen by athermal solvent and a constant approach rate, they concluded that the static force laws are applicable for velocities lower than $V_z \sim kT/\eta R\xi$. Here, η is the solvent viscosity, R is the radius of curvature of the spherical "tip", and $\xi \approx \Sigma^{1/2}$ is the blob size within the Alexander model assuming a steplike concentration profile.[34] Applying their results to colloidal tips, utilizing typical values of $T = 300$ K, $\eta = 10^{-2}$ P, $\xi = 1$ nm, and $R = 15\ \mu$m leads to V_z of the order of 10^{-2} cm/s. To our knowledge, there is no similar analysis for the case of sharp tips. In this last case, it is necessary to estimate the relevant equilibration time of the brush. The perturbation due the insertion of a sharp tip is local. It affects a small number of chains, and it does not affect the chain trajectory as a whole. A full analysis of this problem is beyond the scope of this paper, and we limit ourselves to an intuitive conjecture. To this end, we consider a cylindrical tip immersed in a brush swollen by athermal solvent and described by the Alexander model. In this situation, one may argue that the tip perturbs chain segments of span R_{cyl} comprising $n_b \simeq (R_{cyl}/\xi)^2$ blobs. The associated relaxation time, allowing the chain segment to diffuse a distance R_{cyl}, is[39]

$$\tau_s \simeq n_b^2 \tau_\xi \simeq \left(\frac{R_{cyl}}{\xi}\right)^4 \tau_\xi \simeq \frac{\eta R_{cyl}^4}{\xi kT} \qquad (14)$$

where $\tau_\xi \simeq \eta\xi^3/kT$ is the Zimm time[36] of the blob. The insertion of the tip does not perturb the equilibrium when the approach rate is slow enough, suggesting that the time for displacing the apex by R_{cyl} is long compared to τ_s or that the approach velocity is lower than $V_s \simeq R_{cyl}/\tau_s$. For $T = 300$ K, $\eta = 10^{-2}$ P, $\xi = 1$ nm, and $R_{cyl} = 1$ nm, corresponding to a SWNT, eq 14 leads to $\tau_s \simeq 10^{-9}$ s and $V_s \simeq 10^2$ cm/s. Altogether, the above considerations suggest that thermodynamic force laws apply for low but attainable approach velocities. However, the applicability of the static insertion mode force laws also depends on the form of the tip. For pyramidal probes with a wide half-cone angle, they may be realized only for shallow penetrations since for deep insertions the span of the perturbed region can be larger than H_0. On the other hand, the sharp tip force profiles are expected to describe CNT tips at both shallow and deep insertions. This is of interest because the insertion force profile affords a superior discriminatory power as illustrated by the signatures of the Alexander model and the SCF theory, models that are harder to distinguish in the compression mode. In considering such experiments, it is necessary to allow for two additional points: One is the tilt angle of the CNT with respect to the central axis of the probe. Second, the force scale depends on $A_i^0\Pi_0$ or $A_i^\Theta\Pi_\Theta$, while Π_0 and Π_Θ increases with the grafting density. Accordingly, for sparse brushes, it may be necessary to utilize multiwalled nanotubes or bundles of SWNTs, with a larger cross section.

Acknowledgment. E.B.Z. thanks the UJF and the CNRS for financial support and the LSP for hospitality in Grenoble.

(41) Fredrickson, G. H.; Pincus, P. *Langmuir* **1991**, *7*, 786–795.

Appendix I: The Compression Force within the Self Consistent Field Theory of Brushes

The primary aim of this Appendix is the discussion of the SCF compressive force law in terms of Π for marginal and Θ solvents. It also provides a brief summary of the SCF theory[31] leading to eqs 3 and 4. Within the SCF theory, the free energy per chain in the brush is

$$\frac{F_{\rm chain}}{kT} = \frac{F_{\rm elastic}}{kT} + \frac{F_{\rm inter}}{kT} = \frac{3}{2pa^2}\int_0^H g(h)\,{\rm d}h \int_0^h E(h,z)\,{\rm d}z + \Sigma\int_0^H f_{\rm inter}[\phi(z)]\,{\rm d}z \tag{15}$$

The first term allows for the elastic free energy while the second reflects the contribution due to monomer−monomer interactions. In the elastic free energy, $E(h,z) = {\rm d}z/{\rm d}n$ is proportional to the local tension at z when the chain end is at h, $(3kT/pa^2)E(h,z)$, and $g(h)$ is the distribution function of the altitude of the free ends, h. The average tension per unit area at altitude z, $T_n(z)$, is thus

$$T_n(z) = \frac{3kT}{pa^2\Sigma}\int_z^H E(h,z)\,g(h)\,{\rm d}h \tag{16}$$

The interaction free energy giving rise to the second term is specified in terms of the free energy density $kTf_{\rm inter}[\phi(z)]$ given by the virial expansion $f_{\rm inter}[\phi(z)]a^3 = \tau\phi^2(z) + w\phi(z)^3 + ...$ Within the strong stretching approximation, only chains with $h \geq z$ contribute to $\phi(z)$ and the three unknown functions that specify the brush are thus related via

$$\phi(z) = \frac{a^3}{\Sigma}\int_z^H \frac{g(h)}{E(h,z)}\,{\rm d}h \tag{17}$$

The brush properties are determined by minimization of $F_{\rm chain}$ subject to two constraints

$$\int_0^h \frac{{\rm d}z}{E(h,z)} = N \tag{18}$$

and

$$\frac{\Sigma}{a^3}\int_0^H \phi(z)\,{\rm d}z = N \tag{19}$$

The minimization leads to two key equations

$$E(h,z) = \frac{\pi}{2N}\sqrt{h^2 - z^2} \tag{20}$$

and

$$\frac{a^3\delta f_{\rm inter}}{\delta\phi} \equiv U(z) = \Lambda - \frac{3\pi^2}{8pa^2N^2}z^2 \tag{21}$$

Once Λ is determined via the constraint 19, this last equation leads to solutions for $\phi(z)$ in particular cases such as confined or free brushes in marginal solvent, when $\delta f_{\rm inter}/\delta\phi = 2\tau\phi/a^3$, or in a Θ solvent, when $\delta f_{\rm inter}/\delta\phi = 3w\phi^2/a^3$. In the following, we follow a somewhat different route and first utilize eqs 20 and 21 to express the equilibrium $F_{\rm elastic}$ and $F_{\rm chain}$ as functions of ϕ and the yet unknown Λ.

To this end, we now introduce an elastic free energy density $kTf_{\rm elastic}(z)$ such that $F_{\rm elastic} = kT\Sigma\int_0^{\rm H} f_{\rm elastic}({\rm z})\,{\rm d}z$ or

$$f_{\rm elastic} = \frac{3}{2pa^2\Sigma}\int_z^H E(h,z)\,g(h)\,{\rm d}h = \frac{3\pi}{4Npa^2\Sigma}\int_z^H \sqrt{h^2 - z^2}g(h)\,{\rm d}h = \frac{T_n(z)}{2kT} \tag{22}$$

Substituting eq 20 into $F_{\rm elastic}$ as defined in eq 15 leads to

$$\frac{F_{\rm elastic}}{kT} = \frac{3\pi}{4Npa^2}\int_0^H g(h)\,{\rm d}h\int_0^h \sqrt{h^2 - z^2}\,{\rm d}z = \frac{3\pi}{4Npa^2}\int_0^H {\rm d}z\int_z^H g(h)\sqrt{h^2 - z^2}\,{\rm d}h \tag{23}$$

To express $f_{\rm elastic}(z)$ as a function of $\phi(z)$ and z, we first obtain

$$\frac{{\rm d}f_{\rm elastic}}{{\rm d}z} = -\frac{3\pi}{4Npa^2\Sigma}z\int_z^H \frac{g(h)}{\sqrt{h^2 - z^2}}\,{\rm d}h = -\frac{3\pi^2}{8N^2pa^5}z\phi(z) \tag{24}$$

thus leading to

$$f_{\rm elastic}(z) = -\int_z^H \frac{{\rm d}f_{\rm elastic}}{{\rm d}t}\,{\rm d}t = \frac{3\pi^2}{8N^2pa^5}\int_z^H t\phi(t)\,{\rm d}t \tag{25}$$

which recovers eq 24 upon taking the derivative and satisfies the requirement that $f_{\rm elastic} = 0$ at $z = H$. Noting the similarity between the RHS of eq 25 and ${\rm d}U/{\rm d}z$ as given by eq 21, together with $U(z) = a^3\delta f_{\rm inter}/\delta\phi$ and $\int_z^H U(z)\,{\rm d}\phi = a^3\int_z^H {\rm d}f_{\rm inter}$ leads to

$$a^3 f_{\rm elastic}(z) = -\frac{1}{2}\int_z^H {\rm d}U(t)\,\phi(t) = \frac{1}{2}U(z)\,\phi(z) - \frac{1}{2}U(H)\,\phi(H) + \frac{1}{2}\int_z^H U(t)\,{\rm d}\phi(t) = \frac{\Pi(z)a^3}{2kT} - \frac{\Pi(H)a^3}{2kT} \tag{26}$$

For a free brush at equilibrium, when $\Pi(H) = 0$, this ensures the local force balance, $\Pi(z) = T_{\rm n}(z)$. Utilizing eq 25 leads to

$$\frac{F_{\rm elastic}}{kT} = \Sigma\int_0^H f_{\rm elastic}(z)\,{\rm d}z = \frac{3\pi^2\Sigma}{8N^2pa^5}\int_0^H t\phi(t)\,{\rm d}t\int_0^t {\rm d}z = \frac{3\pi^2\Sigma}{8N^2pa^5}\int_0^H z^2\phi(z)\,{\rm d}z \tag{27}$$

where the RHS is obtained upon changing the order of integration with respect to z and t. Substitution of $(3\pi^2/8Npa^2)z^2 = \Lambda - a^3\delta f_{\rm inter}/\delta\phi$, as obtained from 21, leads to

$$\frac{F_{\rm elastic}}{kT} = \Sigma\int_0^H \left(\frac{\Lambda}{a^3} - \frac{\delta f_{\rm inter}}{\delta\phi}\right)\phi(z)\,{\rm d}z \tag{28}$$

and

$$\frac{F_{\rm chain}}{kT} = \Sigma\int_0^H \left[\left(\frac{\Lambda}{a^3} - \frac{\delta f_{\rm inter}}{\delta\phi}\right)\phi(z) + f_{\rm inter}\right]{\rm d}z$$

$$= \Sigma\int_0^H \left[\frac{\Lambda\phi(z)}{a^3} - \frac{\Pi}{kT}\right]{\rm d}z = \Lambda N - \Sigma\int_0^H \frac{\Pi(z)}{kT}\,{\rm d}z \qquad (29)$$

since $\Sigma\int_0^H\phi(z)\,{\rm d}z = Na^3$ and $\Pi(z)/kT = \phi\delta f_{\rm inter}/\delta\phi - f_{\rm inter}$. The pressure exerted by a brush compressed by a planar surface at altitude $z = H < H_0$ is

$$P_{\rm planar} = -\frac{\partial F_{\rm chain}}{\Sigma\partial H}$$

$$= -kT\frac{N}{\Sigma}\frac{\partial\Lambda(H)}{\partial H} + \Pi(H) + \int_0^H \frac{\partial\Pi(z)}{\partial H}\,{\rm d}z \qquad (30)$$

Equation 21 leads however to $\partial\Lambda/\partial H = (a^3\delta^2 f_{\rm inter}/\delta\phi^2)(\partial\phi/\partial H)$ while $\Pi/kT = \phi\delta f_{\rm inter}/\delta\phi - f_{\rm inter}$ leads to $\partial\Pi/kT\partial H = \phi\delta^2 f_{\rm inter}/\delta\phi^2)(\delta\phi/\delta H)$ and $\partial\Pi(z)/kT\partial H = \phi(z,H)[\partial\Lambda(H)/a^3\partial H]$. Since for a confined brush $\int_0^H\phi\,{\rm d}z = Na^3/\Sigma$, the first term in eq 30 cancels with the last and

$$P_{\rm planar} = \Pi[\phi_{\rm confined}(H)] \qquad (31)$$

To find an explicit force law, it is necessary to invoke a specific choice of $f_{\rm inter}$ and use it to obtain the corresponding $\phi(H)$. Thus, for a marginal solvent, when $\delta f_{\rm inter}/\delta\phi = 2\tau\phi/a^3$, eq 21 assumes the form $\phi(z) = \Lambda_0 - (3\pi^2/16\tau pa^2N^2)z^2$, leading to eq 3 once Λ_0 is specified by eq 19. For a brush confined by a planar boundary at $z = H < H_0$, this leads to

$$\Lambda_0(H) = \frac{Na^3}{\Sigma H} + \frac{\pi^2}{16\tau pa^2N^2}H^2 \qquad (32)$$

and, upon defining $t = H/H_0$ and $y = z/H_0$, to

$$\phi(z,H) = \frac{Na^3}{\Sigma H_0}\left[\frac{1}{t} + \frac{1}{2}(t^2 - 3y^2)\right] \qquad (33)$$

This in turn yields

$$\phi(H) = \frac{Na^3}{\Sigma H_0}\left(\frac{1}{t} - t^2\right) \qquad (34)$$

which upon substitution in $\Pi a^3/kT = \tau\phi^2$ leads to eq 11.

For a Θ solvent, when $\delta f_{\rm inter}/\delta\phi = 3w\phi^2/a^3$, eq 21 assumes the form $\phi(z) = [\Lambda_\Theta - (\pi^2/8wpa^2N^2)z^2]^{1/2}$. For an unconfined layer, utilizing $\phi(H_\Theta) = 0$ and eq 19 leads to

$$\Lambda_\Theta = \frac{\pi^2}{8wpa^2N^2}H_\Theta^2 = \left(\frac{2}{wp}\right)^{1/2}\frac{a^2}{\Sigma} \qquad (35)$$

and H_Θ as given in eq 3. For a layer confined by a planar boundary at $H < H_\Theta$

$$\phi(z) = \sqrt{\Lambda_\Theta(H) - \frac{\pi^2}{8wpa^2N^2}z^2} = \sqrt{\Lambda_\Theta}\sqrt{u^2t_\Theta^2 - y_\Theta^2} \qquad (36)$$

where $t_\Theta = H/H_\Theta$, $y_\Theta = z/H_\Theta$ and $u = (H_\Theta/H)[\Lambda_\Theta(H)/\Lambda_\Theta]^{1/2} = t_\Theta^{-1}[\Lambda_\Theta({\rm H})/\Lambda_\Theta]^{1/2}$. Accordingly, eq 19 assumes the form

$$\int_0^{t_\Theta}\sqrt{u^2t_\Theta^2 - y_\Theta^2}\,{\rm d}y_\Theta = \frac{a^2}{\Sigma}\frac{Na}{H_\Theta\sqrt{\Lambda_\Theta}} = \frac{4}{\pi} \qquad (37)$$

leading to, upon utilizing $\arctan x = \arcsin x/(x^2+1)^{1/2}$, to

$$\frac{\pi}{2t_\Theta^2} = \sqrt{u^2-1} + u^2\arcsin\frac{1}{u} \qquad (38)$$

Numerical solution of eq 38 for a given H and q_Θ yields the corresponding $\Lambda_\Theta(H)$, thus specifying $\phi(z)$ and allowing one to calculate $P_{\rm planar}$ using eq 31.

Appendix II : $F_{\rm ins}$ within the Alexander Model

While the Alexander model[34] yields qualitatively wrong force profiles, its simplicity allows one to gain insights concerning $F_{\rm ins}$ associated with the insertion of a tip of volume $V_{\rm tip}$ into a brush. Although the form of $F_{\rm ins} = \Pi V_{\rm tip}$ is identical to the corresponding bulk penalty, the underlying physics is not. Two points deserve attention: One concerns the physical interpretation of $F_{\rm ins} = \Pi V_{\rm tip}$. As noted in the text, Π is actually the lateral pressure rather than the osmotic pressure of the brush. The second concerns the physical origin of the insertion penalty. In contrast to bulk solutions, it is due to both elasticity and monomer−monomer interactions.

In the Alexander model, the monomer concentration profile is steplike and all chain ends straddle the brush boundary. The free energy per chain comprises two contributions $F_{\rm chain} = F_{\rm elastic} + F_{\rm inter}$ corresponding to the elastic penalty incurred because of the chain stretching and to monomer−monomer interactions. In the mean field regime, the chain exhibits Gaussian statistics and $F_{\rm elastic}/kT \simeq H^2/Na^2$, where N is the polymerization degree and a is the monomer diameter. The interaction free energy is $F_{\rm inter} = kT\Sigma Hf_{\rm inter}$, where $kTf_{\rm inter}a^3 \simeq \tau\phi^2 + w\phi^3$ is the MF interaction free energy density. In the following, we will mostly consider the marginal solvent case $f_{\rm inter}a^3 \simeq \tau\phi^2$. In athermal solvents, the Gaussian elasticity of a chain of blobs is $F_{\rm elastic}/kT \simeq H^2/\phi^{-1/4}Na^2$ while the corresponding interaction free energy $kTf_{\rm inter}a^3 \simeq \phi^{9/4}$. We first discuss the "osmotic pressures" of the brush, distinguishing between $\Pi = -\partial F_{\rm inter}/\Sigma\partial H|_{\Sigma={\rm const}}$, the normal pressure $\Pi_{\rm norm} = -\partial F_{\rm chain}/\Sigma\partial H|_{\Sigma={\rm const}}$, and the lateral pressure $\Pi_{\rm lat} = -\partial F_{\rm chain}^{\rm eq}/H_{\rm eq}\partial\Sigma|_{H=H_{\rm eq}}$. For this purpose, it is essential to keep track of numerical factors arising from differentiation. The equilibrium condition, $\partial F_{\rm chain}/\partial H = 0$, for a marginal solvent leads to $H_{\rm eq}/a = (\tau/2)^{1/3}N(a^2/\Sigma)^{1/3}$, $\phi_{\rm eq} = (2/\tau)^{1/3}(a^2/\Sigma)^{2/3}$ and $F_{\rm chain}^{\rm eq}/kT = 3(\tau/2)^{2/3}N(a^2/\Sigma)^{2/3}$. The condition $\partial F_{\rm chain}/\partial H = 0$ is equivalent to $\Pi_{\rm norm} = T_{\rm n} - \Pi = 0$, where $T_{\rm n}$ is the normal tension per unit area in the brush. The force balance at equilibrium, $T_{\rm n} = \Pi$, leads to $\Pi a^3/kT = \tau\phi_{\rm eq}{}^2 = \tau^{1/3}2^{2/3}(a^2/\Sigma)^{4/3}$ and $\Pi_{\rm lat} = \Pi$. In athermal solvent, the equilibrium condition, $\partial F_{\rm chain}/\partial H = 0$, leads to $H_{\rm eq}/a = (5/7)^{1/3}N(a^2/\Sigma)^{1/3}$, $\phi_{\rm eq} = (7/5)^{1/3}(a^2/\Sigma)^{2/3}$ and $F_{\rm chain}^{\rm eq}/kT = (12/7)(7/5)^{5/12}N(a^2/\Sigma)^{5/6}$. Again, $\partial F_{\rm chain}/\partial H = 0$ implies $\Pi_{\rm norm} = T_{\rm n} - \Pi = 0$, and the force balance at equilibrium $T_{\rm n} = \Pi$ leads to $\Pi a^3/kT = (5/4)\phi_{\rm eq}^{9/4} = (5/4)(7/5)^{3/4}(a^2/\Sigma)^{3/2}$. However, in contrast to the marginal solvent case, for athermal solvents $\Pi_{\rm lat} = (8/7)\Pi$ as discussed in ref 30 in a somewhat different language.

To explore the physical origins of $F_{\rm ins}$, we consider a tip of constant cross section $A_{\rm tip}$ fully inserted into a brush of laterally mobile chains having a total surface area $S_{\rm T}$. The tip is fully immersed; that is, its total length is larger than the equilibrium brush height and its inserted volume is thus $A_{\rm tip}H_{\rm eq} = V_{\rm tip}$. The area per chain of the unperturbed brush is Σ_i while after tip insertion

$S_T - A_{tip} = (S_T/\Sigma_i)\Sigma_f$, thus leading to a smaller area per chain $\Sigma_f = \Sigma_i(1 - A_{tip}/S_T)$. The insertion free energy is

$$F_{ins} = \frac{S_T}{\Sigma_i}\left[F_{eq}(\Sigma_f) - F_{eq}(\Sigma_i)\right] \tag{39}$$

In the limit of large S_T, we may approximate $[(a^2/\Sigma_f)^m - (a^2/\Sigma_i)^m] \approx (a^2/\Sigma_i)^m m(A_{tip}/S_T)$ and since $A_{tip}H_{eq} = V_{tip}$ we obtain

$$\frac{F_{ins}}{kT} = \begin{cases} \dfrac{S_T}{\Sigma_i} 3\left(\dfrac{\tau}{2}\right)^{2/3} N\left[\left(\dfrac{a^2}{\Sigma_f}\right)^{2/3} - \left(\dfrac{a^2}{\Sigma_i}\right)^{2/3}\right] = \dfrac{\Pi V_{tip}}{kT} \\ \quad \text{marginal solvent} \\ \dfrac{S_T}{\Sigma_i}\dfrac{12}{7}\left(\dfrac{7}{5}\right)^{5/12} N\left[\left(\dfrac{a^2}{\Sigma_f}\right)^{5/6} - \left(\dfrac{a^2}{\Sigma_i}\right)^{5/6}\right] = \dfrac{8}{7}\dfrac{\Pi V_{tip}}{kT} \\ \quad \text{athermal solvent} \end{cases} \tag{40}$$

thus suggesting $F_{ins} = \Pi_{lat} V_{tip}$. In this simplified case, F_{ins} is due to uniform lateral compression of the brush, thus giving rise an increase in both $F_{elastic}$ and F_{inter}. For partial insertion and for brushes with immobile head groups, the perturbation of the brush is not uniform. However, in every case, F_{ins} reflects both elastic and interaction contributions.

Appendix III: Conical and a Paraboloid Tips

A cone with a half-angle θ having its apex at altitude $z = D$ has a radius $r(z) = (z - D)\tan\theta$ at altitude z. Accordingly, $A_{cone}(z) = \pi(z - D)^2 \tan^2\theta$, and the insertion force on a conical tip is

$$f_{ins} = 2A^i_{cone}\Pi_i \int_{q_i}^{1} (1 - y_i^2)^{n_i}(y_i - q_i)\, dy_i \tag{41}$$

where $i = 0, \Theta$ and $y_0 = z/H_0$, $y_\Theta = z/H_\Theta$ $q_0 = D/H_\Theta$ with $n_0 = 2$ and $n_\Theta = 3/2$, leading to the upper lines in eqs 9 and 10. A paraboloid tip with its apex at $z = D$ is specified by $z - D = r^2(z)/2R$, where R is the radius of curvature at the apex, $z = 0$. Accordingly, $r(z) = [2R(z - D)]^{1/2}$ and $A_{para}(z) = 2\pi R(z - D)$, thus yielding

$$f_{ins} = A^i_{para}\Pi_i \int_{q_i}^{1} \left(1 - {y_i}^2\right)^{n_i} dy_i \tag{42}$$

leading to the lower lines in eqs 9 and 10.

For a cone, $dr(z) = \tan\theta\, dz$ and $dA(z) = 2\pi(z - D)\tan^2\theta\, dz$. The compressive force on a conical tip in a marginal solvent is thus

$$f_{comp} = 2A^0_{cone}P_0 \int_{q_0}^{1} (y_0 - q_0)\left(\frac{1}{y_0} - {y_0}^2\right) dy_0 \tag{43}$$

For a paraboloid, $dz/dr = r/R$ and $dA(z) = 2\pi R\, dz$. The compressive force on a paraboloid tip inserted into a brush swollen by a marginal solvent is accordingly

$$f_{comp} = A^0_{para}P_0 \int_{q_0}^{1} \left(\frac{1}{y_0} - {y_0}^2\right) dy_0 \tag{44}$$